Oxygen Fugacities of Lavas from the Galapagos Islands and the Galapagos Spreading Center

A Senior Honors Thesis

Presented in Partial Fulfillment of the Requirements for graduation *with distinction* in Geological Sciences in the undergraduate colleges of The Ohio State University

by

Sarah E. Rilling

The Ohio State University
May 2005

MBarton

Dr. Michael Barton
Advisor

Acknowledgements

I would like to thank my parents and family for always being supportive of my interests. Many graduate students and faculty have helped me with technical questions and also all the deadlines and formatting issues I have run into. Thank you to Dr. Barton, for all of the advice and instruction. I appreciate being encouraged to work on undergraduate research, especially to reach beyond topics normally seen in undergraduate classes.

Table of Contents

Abstract

Oxygen fugacity is one of the most important intensive variables that controls the phase relations and compositions of precipitating minerals. It is accepted that oxygen fugacity reflects the redox state of the mantle source region. Therefore oxygen fugacities can be used to probe the mantle redox state and determine mantle heterogeneity. Plume-related magmas and mid-ocean ridge basalts (MORB) have been shown to fall within the same range (ΔFMQ = -1.305 to 0.402) suggesting source regions with similar redox states.

The Galapagos Islands are a result of plume-related volcanoes and located on thin, young crust created by the nearby Galapagos Spreading Center (GSC). This study focuses on the differences between the redox state of the Galapagos plume related magmas and the nearby GSC. The Galapagos Islands show unusually high iron concentrations, which should be reflected in the fO_2 values of lavas. Values of fO_2 calculated from Fe_2O_3/FeO ratios for GSC lavas ranged from ΔFMQ = -1.801 to 0.402. Values calculated from coexisting olivine and melts show excellent agreement with a range of ΔFMQ = -1.818 to 0.069. There is reasonable correlation between oxygen fugacity and *Mg,* consistent with the idea of crystallization controlling oxygen fugacity.

Oxygen fugacities were calculated from coexisting olivine and melt samples from Roca Redonda, Fernandina, and Volcan Darwin on the Galapagos Archipelago. Melt samples were based on groundmass analyses rather than glasses. The results ranged from ΔFMQ = -1.962 to -0.059, similar to values for MORB from the GSC, despite the unusually high $Fe_{8.0}$ and low $Si_{8.0}$ contents. The latter have been used to suggest that the island magmas are generated at greater depths than MORBs.

This study supports other work suggesting that OIB from deeper mantle sources have similar oxygen fugacities to MORB from upper mantle sources. This suggests that both sources have similar redox states, or that differences are not observed in oxygen fugacities of magmas originating from these sources. In the case of the Galapagos Islands this is surprising, given other evidence for differences in melting temperature and depth and source region composition.

I. Introduction

Hans Eugster introduced the concept of oxygen fugacity in 1956 as a thermodynamic term to describe the concept of partial pressure of oxygen (Frost 1991). The effect of varying oxygen fugacity on magmatic processes, mineral stabilities, and mineral and melt compositions igneous rocks has been studied extensively. Variations in oxygen fugacity have been shown to control the crystallization sequence and compositions of solids precipitating from magmas (Carmichael and Ghiorso 1986). In addition, the redox states of magmas reflect that of mantle source regions, and therefore studies of magmas may be used to constrain both the present and past redox states of the mantle (Christie et al 1986).

Buffers originally were designed to control the oxygen fugacity in experimental charges, such that a constant oxygen fugacity is imposed on the experimental charge (Frost 1991). Under natural conditions, the f_{O2} of magmas is a function of primary melt composition (including X_{Fe2O3}/X_{FeO}) and of mineral equilibria during crystallization (Frost 1991). Frost summarized data for many of the buffers used in experimental petrology, and four of these cover the range important for crystallization in natural systems, which can vary by up to seven or eight orders of magnitude for basic lavas (Carmichael 1991). These buffers are:

Low fO_2	$Fe_2SiO_4 = 2Fe + SiO_2 + O_2$	QIF
↓	$2Fe_3O_4 + 3SiO_2 = 3Fe_2SiO_4 + O_2$	FMQ
↓	$2NiO = 2Ni + O_2$	NNO
High fO_2	$6Fe_2O_3 = 4Fe_3O_4 + O_2$	MH

The buffer reactions illustrate how oxygen fugacity reflects of the amount of free oxygen in a system – that is, the amount of oxygen available for chemical reactions. Varying fO_2 drives the reactions in different directions and affects the stability of different minerals. At low fO_2 (fO_2 $\leq$FMQ, or $\Delta FMQ = \log fO_2\,(sample) - \log fO_2$ (FMQ buffer at same T) = 2.7 to +0.4), iron rich silicates such as fayalite are stable. Crystallization at low oxygen fugacity therefore produces iron-rich silicates, and magmas follow an iron-enrichment trend. At higher fO_2 ($\Delta FMQ = 0$ to +3.3), magnetite becomes stable (Barton personal communication) whereas at the highest values of fO_2, hematite is stable. Crystallization of oxides such as magnetite and/or hematite produces silica-rich liquids, and magmas follow silica enrichment trend during crystallization (Carmichael 1991). In closed systems, residual liquids show an increase in fO_2, which indicates

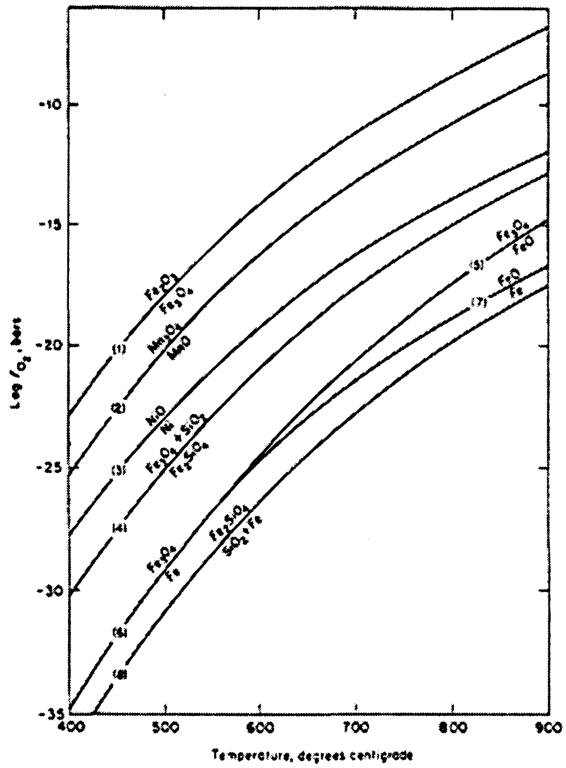

Figure 1 Oxygen buffer assemblages, log*f*O_2 vs T. (1) MH: magnetite-hematite (3) NNO: nickel-nickel oxide (4) QIF: quartz-iron-fayalite (8) FMQ: fayalite-magnetite-quartz
(Igneous Petrology 625, SP2004)

there is an increase in the iron redox state of the liquid during crystallization (Carmichael and Ghiorso 1986).

Although buffers are widely used in experimental petrology, the concept is useful for natural magmas, and the buffers provide reference values of fO_2. The oxygen fugacities of many magmas during crystallization approximately parallel that of one of the buffers described above. Carmichael and Ghiorso (1986) argued that this requires exchange of oxygen between the magma and the surrounding country rock, and they calculated that 0.05g of oxygen must be exchanged for every 100g of magma in order for the latter to stay on the FMQ buffer. The advantage of comparing oxygen fugacities to those of buffers is that the resulting value is independent of temperature (ie. ΔFMQ = logfO_2 (sample)-logfO_2 (FMQ buffer at same T)). The relative oxygen fugacities for compositionally different magmas can then be directly compared and used to infer the redox states of mantle source regions.

Early research suggested that the entire mantle was homogeneous with fO_2 values around the FMQ buffer (ΔFMQ ≈ 0), but mantle xenoliths with oxygen fugacities well below those of the FMQ buffer indicate variations in the redox state of the mantle (Christie et al 1986). Studies of mantle peridotites yield oxygen fugacities ranging from -2.3 to +1.9 ΔFMQ (Barton personal communication.

II. Previous Methods

Several methods are used to determine the oxygen fugacity of lavas, and each method has been found to be limited in its application. The most direct method uses the compositions of magmatic gas sampled during eruptions. The most complete set of measurements available is that from Makaopuhi Lava Lake, Hawaii, which sampled gas emitted during crystallization (Carmichael and Ghiorso 1986). There are relatively few complete sets of magmatic gas analyses, and there is some doubt that oxygen fugacities determined from magmatic gases reflect those of the magmas.

Another method uses the compositions of coexisting Fe-, Ti-oxides (magnetite-ulvospinel and hematite-ilmenite) to determine the oxygen fugacity. This method is based on exchange of Fe^{2+} and Ti between coexisting members of the ulvöspinel-magnetite solid solution series (Fe_2TiO_4-Fe_3O_4) and ilmenite-hematite solid solution series ($FeTiO_3$-Fe_2O_3),

$$\underset{\text{Hematite}}{Fe_2O_3} + \underset{\text{Ulvöspinel}}{Fe_2TiO_4} \leftrightarrow \underset{\text{Ilmenite}}{FeTiO_3} + \underset{\text{Magnetite}}{Fe_3O_4} \quad (1)$$

and the redox equilibrium,

$$\underset{\text{In Ilmenite}}{6Fe_2O_3} \leftrightarrow \underset{\text{In Spinel}}{4Fe_3O_4} + O_2 \quad (2)$$

There are, however, well known limitations on the use of coexisting Fe-Ti oxides to determine fO_2 for igneous rocks. One is the ease with which Fe-Ti oxide compositions are reset by inter-oxide and intra-oxide re-equilibration during cooling or during alteration (eg. Frost, 1991). This severely handicaps the use of coexisting Fe-Ti oxides to determine fO_2 for intrusives and for older igneous rocks, which are more likely to be altered than young rocks. These limitations can be partly or wholly overcome by using assemblages of coexisting ferromagnesian silicates and Fe-Ti oxides to determine fO_2. This approach is predicated on the fact that compositions of Fe-Mg silicates and Fe-Ti oxides are related via equilibria such as

$$\underset{\text{Quartz}}{SiO_2} + \underset{\text{Ulvöspinel}}{2Fe_2TiO_4} \leftrightarrow \underset{\text{Ilmenite}}{2FeTiO_3} + \underset{\text{Fayalite}}{Fe_2SiO_4} \quad (3)$$

termed QUIlF by Frost et al. (1988). This assemblage allows calculation of T and fO_2 from coexisting Fe-Ti oxides as well as from the FMQ equilibrium:

$$\underset{\text{Fayalite}}{3Fe_2SiO_4} + O_2 \leftrightarrow \underset{\text{Magnetite}}{2Fe_3O_4} + \underset{\text{Quartz}}{3SiO_2} \quad (4)$$

Lindsley and Frost (1992) extended the QUIIF equilibrium to magnesian and calcic compositions to include assemblages containing low-Ca and high-Ca pyroxenes. Nevertheless, many igneous rocks, especially many basalts, do not contain coexisting Fe-Ti oxides.

Oxygen fugacity can be also be determined from the redox state of melts. The homogenous reaction

$$\underset{\text{Melt}}{2FeO} + \tfrac{1}{2}O_2 \leftrightarrow \underset{\text{Melt}}{Fe_2O_3} \qquad (5)$$

shows that the ratio $(Fe_2O_3/FeO)^{Melt}$ can be used to calculate fO_2 if the functional relationship between $(Fe_2O_3/FeO)^{Melt}$, fO_2, T, and melt composition is known. Ian Carmichael et al. (1991) have found that the relationship between melt redox state, temperature, and oxygen fugacity can be described by the empirical relation.

$$\ln[X_{Fe2O3}/X_{FeO}] = a\ln f_{O2} + b/T + c + \sum X_i d_I \qquad (6)$$

where a, b, c, d_i are constants found by regression of experimental data. This method is simple, and has the obvious advantage that it can be used for lavas such as primitive basalts that lack mineral assemblages from which fO_2 can be estimated (e.g. MORB). There are, however, potential limitations of the approach. First, it is necessary to determine Fe_2O_3 and FeO by wet chemical or other analytical methods (eg. mössbauer spectroscopy of glasses), techniques not routinely used by petrologists or geochemists. Second, the Fe_2O_3/FeO ratio of rocks is readily affected by alteration, and therefore this method can only be used to estimate fO_2 for unaltered, fresh lavas. In addition, the analyzed Fe_2O_3/FeO ratios of fresh lavas do not necessarily represent those of melts, and hence this ratio should only be used to estimate fO_2 for glassy or aphyric volcanics, or for phyric lavas that do not contain contain cumulate or xenocrystal ferromagnesian minerals.

Given the importance of oxygen fugacity in the petrogenesis of magmas, it would be useful to have additional methods to constrain or determine this variable. In particular, it is desirable to have additional methods to determine fO_2 for basalts, especially ones that contain re-equilibrated Fe-Ti oxides. A method based on olivine-melt equilibrium, is described below.

III. Methods

Two methods were used in this study to calculate oxygen fugacities and the ΔFMQ of lavas. One is based on the relationship between fO_2 and the Fe_2O_3/FeO ratio of melts described earlier, whereas the second method is based on the compositions of coexisting olivine and melt.

1. Oxygen fugacities from Fe_2O_3/FeO ratios

The samples selected for this study were previously analyzed by wet chemistry and electron-microprobe to determine both ferric and ferrous iron concentrations. The full set of glass analyses used in this study was taken from the Ridge Database maintained by Columbia University (http://petdb.ldeo.columbia.edu), and only fresh glasses were selected for this work. In addition, samples from the GEOROC data base (maintained by the Max Planck Institut fur Chimie) for the Galapagos Islands were examined. These samples show wide variations in Fe_2O_3 and FeO that presumably reflects post-eruptive alteration. Because this variation persists even after obviously altered samples (those with high H_2O, alkalies, Rb, and Ba) were eliminated, the samples from the GEOROC data base were not considered further.

Equation 6 was used to determine $\ln fO_2$ from the analyzed Fe_2O_3 and FeO contents of the fresh MORB glasses from the ridge data base. The calculated value of fO_2 was then compared to values for the FMQ and NNO buffers at the same temperature **(assumed to be 1200^{o}C).** All of the samples from the Ridge Database were collected from the Galapagos Ridge, and consist of MORB glasses.

2. Oxygen fugacities from olivine-melt pairs

Oxygen fugacities also were calculated from the compositions of coexisting olivine and melt. This method is based on exchange of MgO and FeO between olivine and basaltic melts, defined as

$$K_D = (X^{Ol}_{FeO}/X^{Melt}_{FeO})(X^{Melt}_{MgO}/X^{Ol}_{MgO}) \tag{7}$$

(X_{MgO} =MgO/[MgO+FeO] on a molar basis). Roeder and Emslie (1970) showed that the exchange distribution coefficient, K_D, is virtually independent of temperature, and that the value is 0.30 ± 03 (1σ) for anhydrous basaltic liquids. Other experimental studies confirm these conclusions for anhydrous basaltic liquids but indicate values of $K_D<0.3$ for evolved melts rich in alkalies (Gee and Sack, 1988). An expression to calculate values of K_D as a function of melt composition is given by Gee and Sack (1988). The relation described by equation 7 has been extensively used by petrologists and geochemists because it allows the equilibrium Fo content of olivine to be predicted from the MgO and FeO contents of any melt, if K_D is known or is calculated as described by Gee and Sack (1988). The experiments of Roeder and Emslie (1970) were conducted over a range of fO_2 ($10^{-0.68}$ to 10^{-12}), and thus indicate that K_D is independent of fO_2, so that the equilibrium composition of olivine can be predicted from the MgO and FeO contents of melts that crystallize over a wide range of fO_2 (ΔFMQ from +7.6 to -3, or from values appropriate for crystallization in air to values near those of the iron-wüstite [IW] buffer). Of course, this does not mean that the composition of olivine in equilibrium with a particular melt remains constant as fO_2 varies. On the contrary, the experiments of Roeder and Emslie (1970) show that the Fo content of olivine in equilibrium with melt of fixed total composition increases with increasing fO_2 at constant T (Fig. 2). Because K_D is independent of fO_2, the apparent correlation between the Fo content of olivine and fO_2 actually reflects the dependence of Fe_2O_3/FeO in the melt on fO_2.

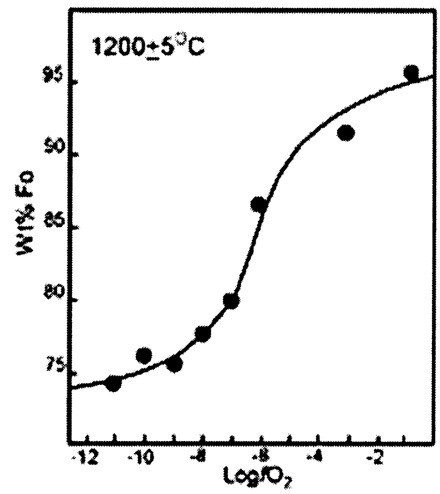

Figure 2 Varying olivine composition with changing oxygen fugacity at constant T. (Roeder and Emslie 1988)

Most petrologists and geochemists recognize that use of equation 7 requires assumptions about the redox state of melts for which Fe_2O_3 and FeO contents have not been determined analytically – which the case in the majority of recent petrological and geochemical studies. In studies of olivine-melt equilibrium it therefore is common practice to adopt an arbitrary value for Fe_2O_3/FeO in melts (e.g. 0.1 or 0.15), or to assume that crystallization occur at some value of fO_2 (e.g..FMQ=0) and then calculate Fe_2O_3 and FeO contents of melts from equation 6. However, it is preferable to use the compositions of coexisting olivine and melt to determine $Fe_2O_3^{Melt}$ and FeO^{Melt} from total (analyzed) Fe, and use these to calculate $\log fO_2$ during crystallization.

The method is illustrated graphically using an example taken from the literature (Figure 3). The analyses of olivine and glass used in this example are from the results of an experiment on a basalt from the East Pacific Rise (ALV-2004-3-1-20) with fO_2 controlled near FMQ (Yang et al. 1996). The olivine and glass produced in the experiment were analyzed by electron microprobe, and total Fe is reported as FeO.

The first step is to calculate fictive melt compositions with variable Fe_2O_3 and FeO contents (wt. %), adjusting all oxide percentages for the change in total mass resulting from addition of oxygen due to the change in the oxidation state of iron. The resulting values of Fe_2O_3 are plotted against calculated values of X^{Melt}_{MgO} (Mg#) in Fig 3a, and the latter are used to calculate the Fo contents (Fo) of olivine in equilibrium with these melts (Fig. 3b), using values of K_D determined from the empirical relationship given by Gee and Sack (1988). Fo is plotted against Fe_2O_3 in Fig. 3c. The actual Fe_2O_3 content of the melt is determined from the known (analyzed) composition of olivine ($Fo_{0.836,}$ Yang et al. 1996), and FeO^L is calculated from total Fe ($FeOT=0.8998Fe_2O_3+FeO$). The values of $Fe_2O_3{}^L$ and FeO^L are used in equation 6 to estimate $\log fO_2$ at the reported run temperature of 1188^oC using the coefficients given by Kress and Carmichael (1991). The agreement between $\log fO_2$ estimated from olivine-melt equilibrium (-8.65) and that given by Yang et al (1996) for this experiment (-8.72) is excellent. In practice, the value of $Fe_2O_3{}^L$ is calculated from regression of $Fe_2O_3{}^L$ versus olivine composition and used to calculate $\log fO_2$. For brevity, this method is hereafter referred to as the olivine-melt oxybarometer.

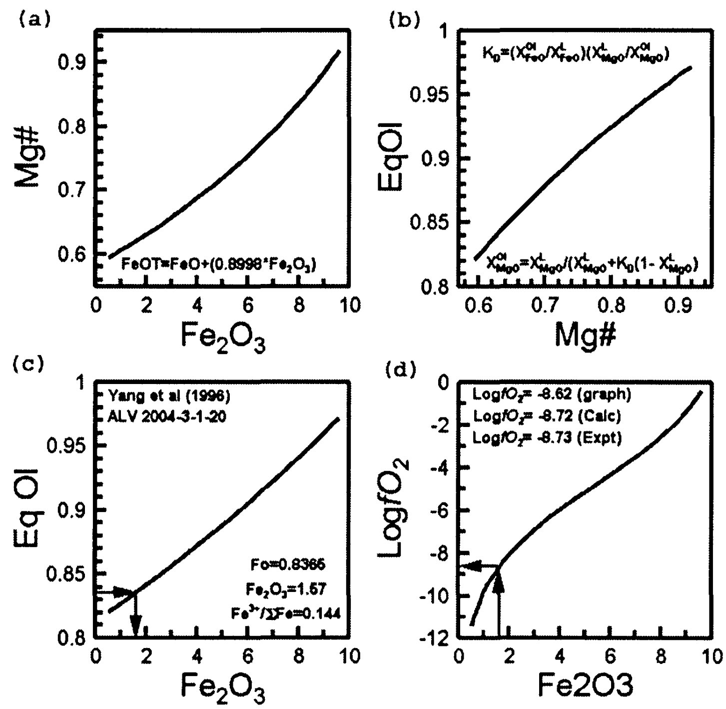

Figure 3 Olivine-melt oxybarometer method. The relationship between olivine and melt compositions is used to determine the oxygen fugacity of magmas as described above. (Adapted from Yant et al 1996, Barton personal communication)

IV. Application to lavas from the Galapagos Ridge and Galapagos Islands

The objective of this research is to determine the oxygen fugacities for crystallization of basaltic magmas along the Galapagos Spreading Center (GSC) and on the Galapagos Islands. The GSC constitutes a divergent margin, and hence oxygen fugacities of these magmas should reflect those of the mantle source beneath the mid ocean ridge system. Volcanism on the Galapagos Islands is widely believed to reflect a plume or hot spot in the underlying mantle, and the oxygen fugacities of these magmas should reflect those of the underlying mantle plume or hot spot source. There is some debate about the existence of mantle plumes in general, but most workers concede that ocean island basalts (OIB) such as those erupted on the Galapagos Islands are derived from a different mantle source than mid ocean ridge basalts (MORB). Therefore, the research described in this study addresses the question of whether the redox states of MORB mantle and OIB mantle are the same or different.

Analyses of coexisting olivines and glasses in samples from the Galapagos Spreading Center and from the Galapagos Islands selected from the literature were used to calculate $\log fO_2$. The latter were compared to values for the FMQ and NNO buffers at the same temperature (assumed to be $1200^{O}C$), and to the values obtained from the analyzed Fe_2O_3/FeO ratio of glasses from the GSC and other ridges.

V. Geologic Background

1. Location

The Galapagos archipelago is a group of volcanic islands located near the Galapagos Spreading Center (GSC), which separates the Cocos and Nazca Plates. Although attributed to plume magmatism on the basis of He isotope studies, the volcanoes of the archipelago do not form the typical linear trend parallel to plate motion like those of the Hawaiian-Emporer Chain, but generally become younger to the west in agreement with plate movement. Volcanism has been active for 5 to 6 My, with earlier activity being split into the Cocos and Carnegie Ridges (Figs. 4, 5) by a serious of ridge jumps (Allan and Simkin 2000). The crust below the islands is young and relatively thin, so the volcanoes are scattered with no one center of activity unlike the Hawaiian Islands (Geist et al 1999). Harpp et al (2003) described the islands as being one of the few places on the globe that exhibit magmatism related to both plume and ridge related mantle processes, but not dominantly one or the other.

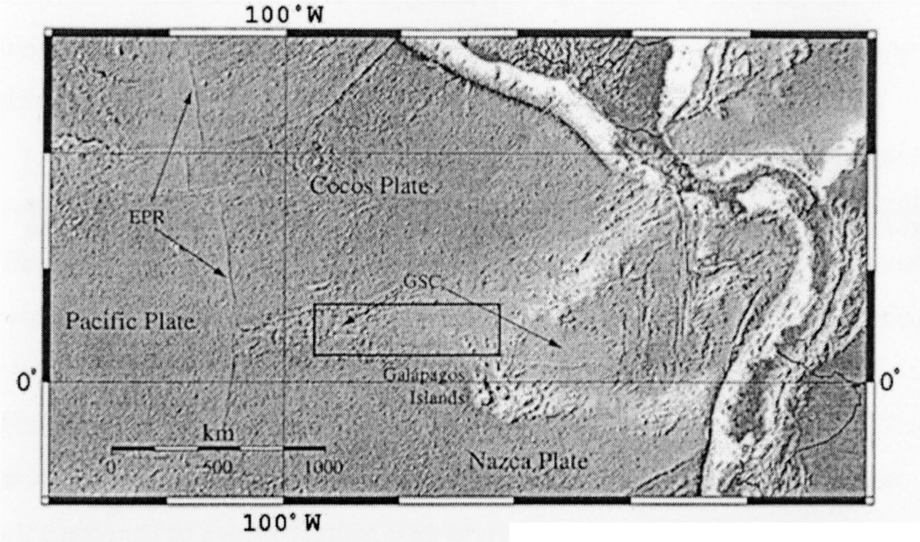

Figure 4 Bathymetric image of the Galapagos region (Cushman et al 2004)

2. Geographic and geochemical variations

Seven major volcanoes form an east-facing horseshoe pattern (Figures 5 and 6). Those in the center of the horseshoe exhibit depleted upper mantle MORB geochemical signatures compared to more enriched lavas occur in the north, west, and south sides of the horseshoe (Harpp and White 2001). Some have suggested that plume material is being sheared to the east by underlying asthenospheric flow and the movement of the Nazca Plate, but that it also is flowing northward toward the GSC, with plume components observed near and in ridge lavas (Harpp and White 2001, Harpp et al 2003). Werner et al (2003) have suggested that the same pattern of enriched domains can be identified in activity over the past 14.5 Mya in the Cocos track. Lavas erupted along the Cocos track, and in the Carnegie, Malpelo, and Coiba ridges all exhibit compositional characteristics that are similar to the current Galapagos hotspot magmas (Werner et al 2003);

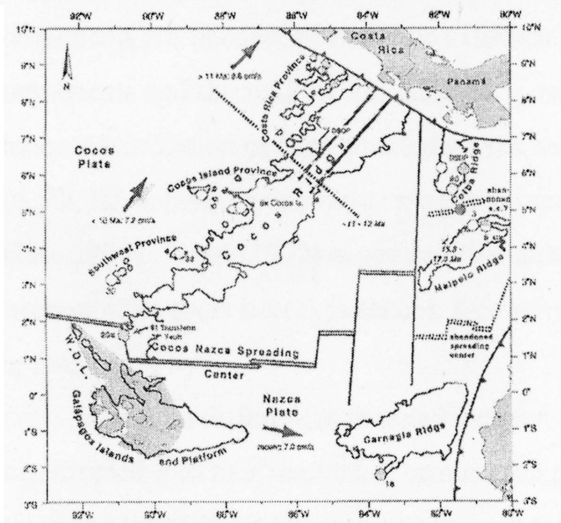

Figure 5 Ancient ridge on the Cocos and Naxa plates from plume activity. Recent Galapagos activity is highlighted. (adapted from Werner et al 2003)

Harpp and White (2001) have suggested that part of the geographic variations may reflect origin from an internally heterogeneous plume with a northern limb different from the southern limb, rather than effects of magma evolution during ascent from the mantle.

Although regional stresses caused by the ridge movement and plume influence are responsible for magma generation and transport, the varying magma compositions likely reflect differences between ridge and plume material (Nusbaum 1991). Compositional variations evident in Sr, Nd, and Pb isotopic data, and in incompatible trace element concentrations, have been attributed to plume-asthenosphere mixing, and to variable depths of partial melting, and different depths of crystal fractionation, especially in the western lavas (Geist 1999). Vulcan Darwin, in particular shows disequilibria between residual melt and xenocrysts, suggesting the melt continued to evolve further after crystallization of the phenocrysts (Nusbaum et al 1991). Isotopic ratios and incompatible element concentrations (corrected for the effects of fractionation) do not correlate, indicating that magma mixing is probably not the dominant process (Geist 1992). Harpp and White (2001) used Pb-Pb variations to show that binary mixing between mantle sources is inadequate to explain compositional variations, and that four components are needed. Most of the evidence supports mixing between various plume components and the shallow asthenosphere, rather than between different plume components alone. Assimilation of lithosphere does not seem to have played a significant role because Sr, Nd, Pb, Hf, and O isotope ratios appear to remain constant during magma evolution (Harpp and White 2001). Geist (1992) suggested that although variation in magma compositions are observed over short lateral distances, they may reflect magma generation at greatly different depths.

Based on differences in geochemistry, and ages of volcanic products, the islands have been divided into four regions. The northern province lies between the inferred current plume center and the GSC and contains volcanoes that erupt plagioclase-rich lavas (Geist 1999). At the northeastern edge of the islands along the GSC there are more seamounts than along any other area of the ridge. Lavas from these seamounts show MORB-like rare earth element (REE) patterns and represent the most light-rare earth element (LREE) depleted material observed in the archipelago. Lavas from the Wolf-Darwin lineament, the northwest islands, also exhibit MORB-like characteristics, but some show slight LREE-enrichment (Harpp and White 2001). Volcanics from this province show evidence for only a small amount of plume component in the mantle source region (Harpp and White 2001). The lowest $^3He/^4He$ ratios of the Galapagos islands has been observed on Pinta (Kurz and Geist 1999).

The southern and western provinces of the islands tend to contain young tholeiitic shield volcanoes (Geist 1992). The lavas on the western islands are thought to have evolved from primitive magma originating from a deep mantle source (Geist 1992). Lavas from Cerro Azul, Sierra Negra, and Floreana have intermediate $^3He/^4He$ ratios associated with high radiogenic isotope values (Kurz and Geist 1999). Some of the Floreana lavas have been explained as asthenosphere material reacting with LREE and volatile enriched fluids (Harpp and White 2001). Mantle metasomatism is supported by the highest values of Sr, Nd, and Pb in the islands, and by the elevated Ba, La, and Th concentrations; additional evidence exists in trace elemental trends, and by the tendency for alkaline lavas to erupt in explosive, pyroclastic events (Harpp and White 2001). Harpp and White (op cit) have suggested that a distinct mantle composition beneath the southwest area explains the localized differences in geochemistry.

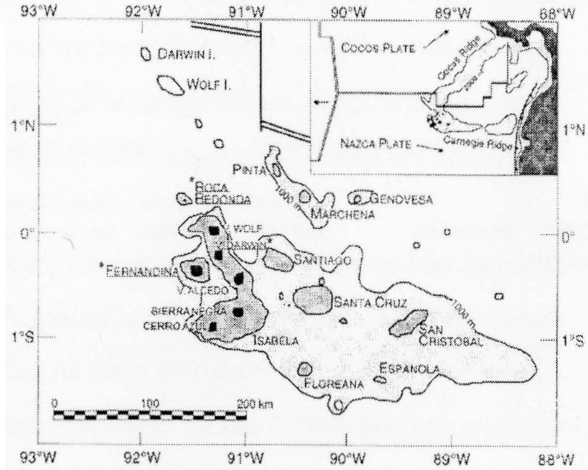

Figure 6 Island and volcano locations in the Galapagos Archipelago (Geist 1992)

Roca Redonda lacks a caldera and is grouped into the western province, but the volcano does not actually lie on the Galapagos platform (Standish et al 1998). Lavas are dominated by plagioclase and olivine phyric types, in which olivine cores range from Fo_{78} to $Fo_{83.5}$, with rims about 12% lower Fo (Standish et al 1998). An average $FeO_{(8.0)}$ of 12.7 is significantly higher than for other volcanoes of the province (Standish et al 1998). The lavas are more degassed than Fernandina and exhibit less evidence of a plume contribution; all lavas are LREE enriched and lie within the alkaline field for Hawaiian basalts on an alkali-silica plot (Standish et al 1998). The samples show more isotopic enrichment than the Wolf-Darwin lineament, so simple plume-ridge mixing can be ruled out as the primary process (Standish et al 1998).

The central province is characterized by lavas exhibiting evidence of more plume component, and more depleted MORB than the surrounding provinces (Geist 1992). The island volcanoes lack calderas, and they erupt alkali-olivine basalt lavas with more diversity than originally expected (Geist 1992). The diversity probably reflects a mantle source containing components of all four regions, but with only small contributions from the southwestern member (Harpp and White 2001). The highest $^3He/^4He$ ratios are from Fernandina, with a steep decline toward the north and east (Kurz and Geist 1999). Source heterogeneity is supported by correlation of the $^3He/^4He$ values with averaged $FeO_{(8.0)}$, $Na_2O_{(8.0)}$, and Nb/La (Kurz and Geist 1999).

Fernandina is believed to represent the purest plume eruptions as evidenced by the high $^3He/^4He$ ratios (Harpp and White 2001). Eruptions generally are small volume Aa flows of hypersthene-normative tholeiites with plagioclase as the most abundant phenocryst (Allan and Simkin 2000). From textural analysis, Cr-rich spinel appears to be the first mineral to crystallize, with Fo-rich olivine also crystallizing early (Allan and Simkin 2000). Most olivine cores range from Fo_{79} to Fo_{84} (Allan and Simkin 2000). The low Mg# and low incompatible element contents indicate the host magma was relatively evolved (Allan and Simkin 2000).

3. Ridge Volcanism

Lavas erupted near the center of the plume and along the GSC exhibit variations in geochemistry greater than shown by lavas erupted along ridges elsewhere in the world. In addition, there are substantial variations in crustal thickness, and morphology. On either side of the Galapagos plume region, the spreading center contains a mid-Atlantic Ridge-like valley (Cushman et al 2004). East of 85°W, and west of 95.5°W, ridge lavas have normal MORB compositions, but the lavas erupted between 85°W and 95.5°W show variable enrichment in LREE and in large ion lithophile elements (LILE) (Cushman et al 2004). GSC lavas that fall in the NMORB field show geographical trends with $FeO_{(8.0)}$ and $TiO_{2(8.0)}$ decreasing and $SiO_{2(8.0)}$ increasing from west to east (Cushman et al 2004). The greatest plume influence is shown by lavas erupted between 91.7°W and 92.4°W were the highest MgO contents are found (Cushman et al 2004).

VI. Results

As mentioned above, samples from the Galapagos Island in the GEOROC database have highly variable compositions reflecting alteration, and they were not used in this project. The oxygen fugacities for samples from the Galapagos Islands were determined using the olivine-melt oxybarometer. These samples are typical basalts with SiO_2 contents between 47.29 and 49.45, an average of 48.57. FeOT concentrations range from 9.37 to 13.78, but ferric iron ratios, $Fe_2O_3/(FeO + Fe_2O_3)$, average 0.129 and range between 0.080 and 0.172. Values for the ΔFMQ were between -1.9617 and -0.0591 with an average of -0.8270. The complete analyses are listed in Appendix 1.

The majority of island samples were taken from Fernandina, which is thought to represent current plume location. Ignoring samples from Volcan Darwin and Roca Redonda, the ferric iron ratio covers a slightly smaller range (0.100 to 0.172), but shows an average of 0.127, similar to the average all island samples. The ΔFMQ for Fernandina has only a slightly lower average at -0.8646.

Oxygen fugacities for GSC samples from the ridge database were calculated from both the analyzed $(Fe_2O_3/FeO)^{Melt}$ and from olivine-melt equilibrium. The results obtained by both methods fall into very similar ranges. SiO_2 contents for ridge database samples average 51.77, and 50.37 for the olivine-melt oxybarometer samples. Ferric iron ratios had a slightly larger range for the ridge database (0.0736-0.1813) than the olivine-melt oxybarometer (0.0828-0.1713), but the averages were very similar: 0.1366 and 0.1354, respectively. ΔFMQ values also had similar averages at -0.4636 and -0.6406. Complete analyses for the ridge database samples are given in Appendix 2, and olivine-melt oxybarometer samples are given in Appendix 3.

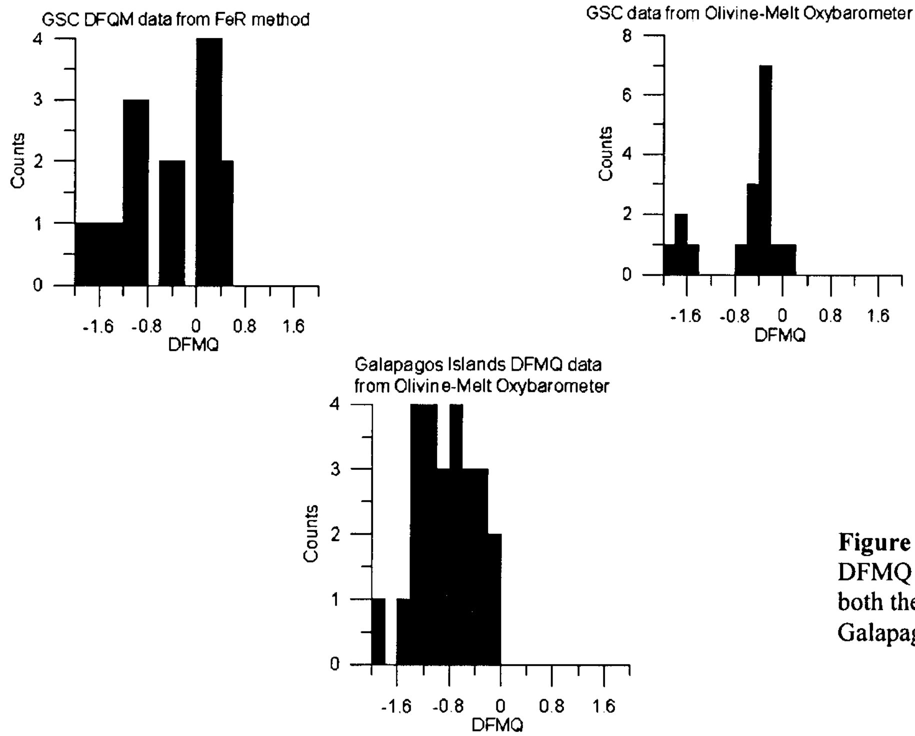

Figure 7 Ranges of DFMQ for data from both the GSC and the Galapagos Islands

VII. Discussion

1. Correlation between ΔFMQ and compositional parameters

Plots of ΔFMQ versus various elements do not reveal consistent trends. SiO2 covers a narrow range and therefore does not correlate with ΔFMQ in the GSC samples. Study of samples with higher silica contents is needed to determine whether any such correlation actually exists, and the same conclusion is valid for samples from the GSC. This may reflect the style of differentiation during crystallization. The magmas follow a typical tholeiitic trend – iron enrichment at near constant silica. However, there is also poor correlation between ΔFMQ and MgO, which normally is an excellent indicator of differentiation. These results imply that magma evolution along the GSC and on the Galapagos Islands is complex and is not simply the result of crystallization. Nevertheless, trends on plots of ΔFMQ versus Mg# suggest that crystallization played some role in magma differentiation. The initial increase in ΔFMQ as Mg# decreases reflects crystallization of silicates such as olivine (±clinopyroxene) so that Fe^{3+} increases in residual liquids until Fe-Ti oxides crystallize whereafter Fe^{3+}decreases in residual liquids. A plot of total iron versus MgO reveals that the GSC samples from the Ridge data base follow a strong iron enrichment (tholeiitic) trend.

Data for the Galapagos Islands also show considerable scatter on many of the plots, which may reflect that fact that few of the samples are glasses – they are mixtures of glass and phenocrysts. However, the array of data on a plot of ΔFMQ versus Mg# is similar to that for GSC samples, confirming the fact that crystallization played some role in magma differentiation.

2. GSC compared to MORB compositions

Compiled data for global MORBs analyzed for $(Fe_2O_3/FeO)^{Melt}$ show a range in ΔFMQ from -2.87 to 0.19, with values for the East Pacific Rise (EPR) between -2.59 and 0.10 (McCann and Barton personal communication). Although a few samples from the GSC fall below these ranges, the average value is almost exactly in the middle. This suggests that the GSC basalts are typical MORB lavas and are not heavily affected by plume magmas; that there is interaction of plume material in the ridge but not substantial enough to affect ΔFMQ; or that interacting mantle plume has a similar fO_2 to mantle beneath the ridge.

	EPR	GSC	OIT	**Galapagos Islands**	Plume MORB (Azores)
SiO2	50.19	**51.19**	50.51	**48.57**	49.72
TiO2	1.77	**1.84**	2.63	**3.20**	1.46
Al2O3	14.86	**13.81**	13.45	**15.78**	15.81
FeOT	11.33	**11.10**	--	**--**	--
FeO	--	**--**	9.59	**9.69**	7.62
Fe2O3	--	**--**	1.78	**1.43**	1.66
MgO	7.10	**6.48**	7.41	**6.01**	7.90
CaO	11.44	**10.75**	11.18	**11.08**	11.84
Na2O	2.66	**2.56**	2.28	**3.11**	2.35
K2O	0.16	**0.19**	1.49	**0.59**	0.50

Table 1 Results compared to Wilson (1989)

Harpp and White (2001) noted that volcanoes in the northwest province of the Galapagos exhibit only slight involvement of a plume component in the mantle sources, which supports the idea of plume material having little or no effect on the MORB fO_2 signatures between the ridge and the islands. However, Cushman et al (2004) showed some plume influence between 91.7°W and 92.4°W, because of high MgO contents and variable $FeO_{(8.0)}$ and $TiO_{2(8.0)}$ that are not seen in other areas of the GSC (2004). Therefore, the influence of the Galapagos plume is seen in both major element and isotope compositions, but an overall difference in fO_2 can not be seen. This suggests that the plume material in the GSC and the typical GSC material share a similar fO_2 signature, even though they come from different mantle source regions.

3. Galapagos Islands versus typical plume magmas

The major element analysis of the Galapagos lavas are more similar to Wilson's (1989) values for typical ocean-island tholeiites (OIT) than for her typical plume-MORB (Azores) for ferrous iron oxides and CaO. However, the are closer to plume-MORBs for SiO_2, Al_2O_3, and K_2O (1989). Concentrations of ferric iron and MgO are lower than both OIT and plume-MORB, but TiO_2 and Na_2O are both significantly higher.

4. Galapagos Islands versus the GSC compositions

Samples from the Galapagos Islands fall mostly within MORB ranges for ΔFMQ but tend to lie in the lower end of the range. The have slightly lower SiO_2 contents than ridge lavas, similar total iron, and slightly lower Fe^{3+}/Fe^{2+} ratios. They exhibit similar average values of MgO (6.48 in the GSC and 6.01 in the islands), but the GSC lavas shows a much greater range in MgO content (from 1.60 to 9.46 compared to 4.89 to 8.86 in island lavas). Results of this study suggest that the GSC and plume source regions are similar, which implies that the redox state is homogenous throughout the asthenosphere and lower mantle. However, it could mean that the redox state is not uniform, but that the plume has reequilibrated with the upper mantle with respect to the redox state.

Geist (1992) has showed that central island lavas are more alkali-olivine tholeiites (specifically, hypersthene- normative tholeiites from Fernandina) which lies above the current plume location. The central lavas also show high He ratios compared to ridge lavas or lavas from island edges (Kurz and Geist 1999). Carmichael (1991) stated that alkali-rich lavas which ascend quickly tend to be the most oxidized, but the plume lavas actually have lower ferric iron ratios than those in the GSC. Elemental and isotopic evidence supports a deeper mantle magma generation for the plume than the upper asthenosphere MORB source of the GSC. This eliminates the possibility that the magmas are generated in the same source regions. Because compositional differences between plume magmas and OIB are obvious, it is difficult to understand how the plume could reequilibrate with the upper mantle, as any such reequilibration should be seen in the concentrations of other elements and in the isotopic data.

The lavas at Roca Redonda are representative of simple plume and ridge magma mixing and they show ΔFMQ values that are even lower than those observed from Fernandina, the presumed center of the plume. If there is a distinctive fO_2 signature from the plume, compared to MORB, the Roca Redonda values should lie between those of the plume and the ridge. If so, this would support the idea of a homogeneous mantle, or that the heterogeneity of the mantle is not manifest in oxygen fugacities. Roca Redonda lavas still clearly shows the signature of plume magmas, which would not be the case if the plume had equilibrated to the upper mantle.

5. Future Work

Although the ΔFMQ values for the Galapagos Islands are slightly lower than the GSC, and normal MORB ranges, they are not statistically different. In part, this may reflect the small number of samples from the Galapagos Islands that were used in this study. Further work should be done to collect fresh samples and analyzed for both ferric and ferrous iron of the lavas. Multiple methods should be used to determine fO_2, for comparison and to determine the true range and average values of the Galapagos plume. Comparison with other mantle plume might also be useful. .

Samples could be collected from all four different geochemical provinces of the Galapagos Islands, rather than only the current plume center, and then compared to see if different proportions of plume material can be observed. The complexity of ridge and plume magmas make interpretations difficult if the structure of the plume is not well understood. The lavas from the Galapagos island have some of the highest iron contents in the world and are located in a warm, moist environment. This makes weathering a major concern and questionable samples need to be carefully examined before they are included in research. Completely fresh samples would help to manage statistical uncertainities, which would be make the data interpretations more reliable.

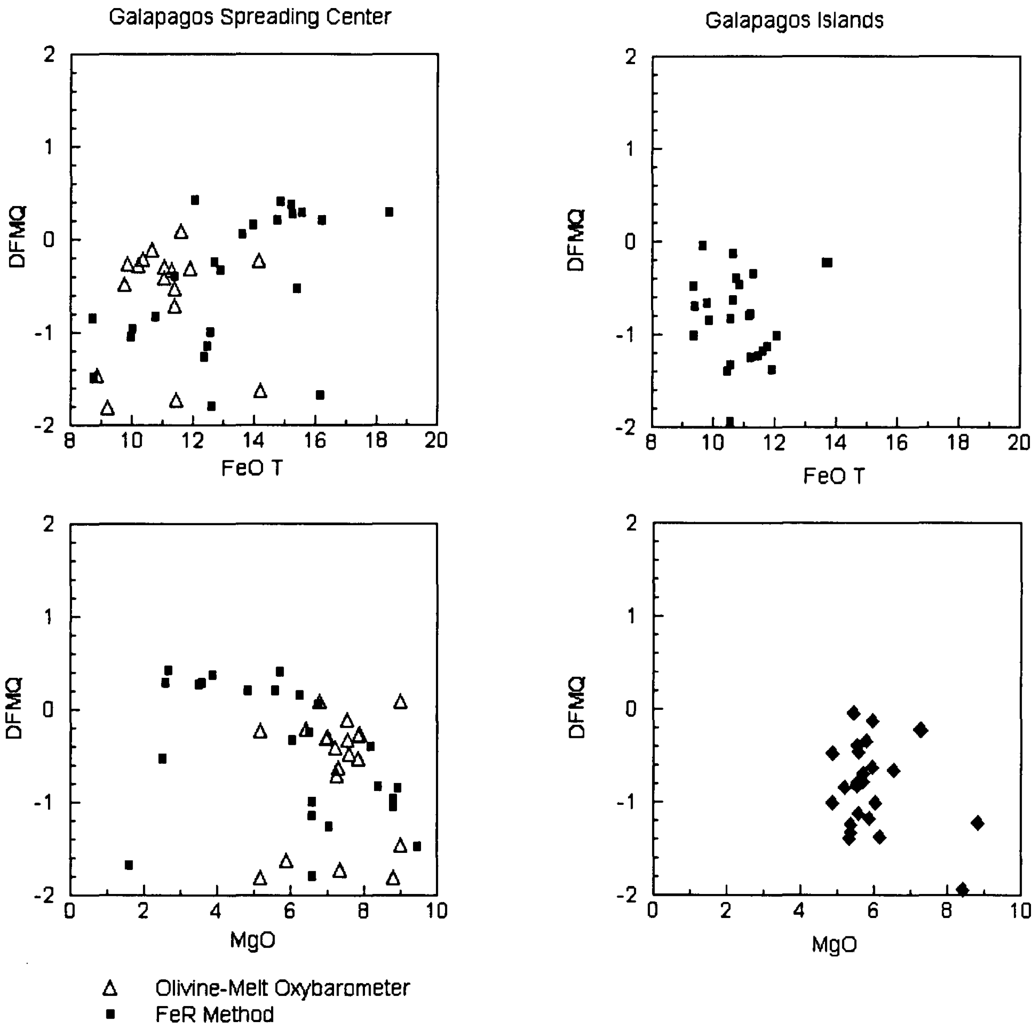

VIII. Conclusion

Samples analyzed with the olivine-melt oxybarometer method have ΔFMQ values which agree with samples analyzed with the traditional ferric-ferrous iron ratio method. The results from these methods are similar for lavas from both the GSC and from the Galapagos Islands, although major and trace element evidence supports different source regions for the lavas-typical upper athenosphere MORB source for the GSC, deep mantle plume source for the Galapagos Islands. There is also evidence of magma mixing and fractionation, causing various geochemical provinces throughout the islands which is not clearly repeated in ΔFMQ values. This does not necessarily support a homogenous mantle, but suggests that the varying source regions can not be accurately identified using fO_2 calculations of only a few samples.

IX. References

Allan, J.A. and Simkin, T. (2000), Fernandina Volcano's evolved, well-mixed basalts: Mineralogical and petrological constraints on the nature of the Galapagos plume, *J. Geophys. Res.,* 105, B3, 6017-6041.

Carmichael, I.S.E. (1991), The redox state of basic and silicic magmas: a reflection of their source regions?, *Contrib. Mineral. Petrol.,* 106, 129-141.

Carmichael, I.S.E., Ghiorso, M.S. (1986), Oxidation-reduction relations in basic magma: a case for homogeneous equilibria, *Earth Planet. Sci. Lett.,* 78, 200-210.

Christie, D.M., Carmichael, I.S.E., and Langmuir, C.H. (1986). Oxidation states of mid-ocean ridge basalt glasses, *Earth Planet. Sci. Lett.,* 79, 397-411.

Cushman, B., Sinton, J., Ito, G., and Dixon, J.E. (2004), Glass compositions, plume-ridge interaction, and hydrous melting along the Galapagos Spreading Center, 90.5°W to 98°W, *Geochem. Geophys. Geosyst.,* 5(8), Q08E17, doi:10.1029/2004GC000709.

Frost, B.R. (1991), Oxide Minerals: Petrologic and Magnetic Significance, *Rev. in Mineral.,* 25.

Frost, B.R. and Lindsley, D.H.(1991), Oxide Minerals: Petrologic and Magnetic Significance, *Rev. in Mineral.,* 25.

Gee and Sack (1988), Experimental petrology of melilite nephelinites, *J. Petrology,* 29, 1233-1255.

Geist, D.J. (1992), An appraisal of melting processes and the Galapagos Hotspot: Major- and trace-element evidence, *J. Volcanol. Geotherm. Res.,* 52, 65-82.

Geist, D., White, W., Naumann, T., and Reynolds R. (1999), Illegitimate magmas of the Galapagos: Insights into mantle mixing and magma transport, *Geology,* 27, 12, 1103-1106.

Harpp, K.S., Fornari, D.J., Geist, D.J., and Kurz, M.D. (2003), Genovesa Submarine Ridge: A manifestation of plume-ridge interaction in the northern Galapagos Islands, *Geochem. Geophys. Geosyst.,* 4(9), 8511, doi:10.1029/2003GC000531.

Harpp, K.S., and White, W.M. (2001), Tracing a mantle plume: Isotopic and trace element variations of Galapagos seamounts, *Geochem. Geophys. Geosyst.*, 2, pn:2000GC000137.

Kress, V.C., and Carmichael, I.S.E. (1991), The compressibility of silicate liquids containing Fe (sub 2) and O (sub 3) and the effect of composition, temperature, and oxygen fugacity and pressure on their redox states, *Contrib. Mineral. Petrol.*, 108(1-2), 82-92.

Kurz, M.D. and Geist, D. (1999), Dynamics of the Galapagos hotspot from helium isotope geochemistry, *Geochim. Cosmochim. Acta,* 63, 4139-4156.

Nusbaum, R.L., Colgan, M.W., Lawton, D.E., and Glascock, M.D. (1991), Mineralogic constraints on the magmatic history of Volcan Darwin flank lava at Urvina Bay, Isla Isabela, Galapagos Islands, *J. Volcanol. Geotherm. Res.*, 47, 359-366.

Roeder and Emslie (1970), Olivine-liquid equilibrium, *Contri. Mineral. Petrol.*, 29, 275-289.

Standish, J., Geist, D., Harpp, K. (1998), The emergence of a Galapagos shield volcano, Roca Redonda, *Contrib. Mineral. Petrol.,* 133, 136-148.

Werner, R., Hoernle, K., Barckhausen, U., and Hauff, F. (2003), Geodynamic evolution of the Galapagos hot spot system (Central East Pacific) over the past 20 m.y.: Constraints from morphology, geochemistry, and magnetic anomalies, *Geochem. Geophys. Geosyst.,* 4(12), 1108, doi:10/1029/2003GC000576.

Wilson, M. (1989), Igneous Petrogenesis: A Global Tectonic Approach.

Yang et al. (1996), Experiments and models of anhydrous basaltic olivine-plagioclase-augite saturated melts from 0.001 to 10 kbar, *Contrib. Mineral. Petrol.*, 124, 1-18.

Ridge Data: Ferric-Ferrous Ratios

	SiO2	Al2O3	TiO2	Fe2O3	FeO	MnO	MgO	CaO	Na2O	K2O	P2O5	TOTAL
KAK1979-011-078	50.00	15.54	0.88	0.84	8.00	0.16	9.46	12.84	1.82	0.04	0.10	99.68
KAK1979-012-040	49.63	15.51	1.02	1.16	8.97	0.19	8.79	12.03	2.15	0.05	0.09	99.59
KAK1979-018-021	50.67	13.81	1.80	1.23	11.26	0.22	7.06	10.99	2.33	0.17	0.17	99.71
KAK1979-012-057	50.78	13.52	1.91	1.87	11.24	0.27	6.08	10.93	2.45	0.20	0.30	99.55
ALV0994-003B	56.21	11.19	2.44	2.61	13.23	0.23	2.59	7.34	2.87	0.41	0.51	99.63
ALV0996-005C	50.64	12.06	2.85	2.70	13.77	0.26	4.86	9.68	2.44	0.23	0.28	99.77
ALV0996-007C	51.09	10.48	3.71	3.07	15.65	0.29	3.61	8.73	2.53	0.28	0.45	99.89
ALV1000-003C	51.63	12.21	2.01	2.27	11.56	0.23	6.77	10.84	2.31	0.15	0.16	100.14
SON0012-159-A	49.91	14.89	1.30	1.31	9.58	0.18	8.38	11.88	2.20	0.13	0.10	99.86
SON0012-143-A	50.05	14.37	1.55	1.62	9.97	0.19	8.18	11.40	2.16	0.18	0.14	99.81
SON0012-130-A1	49.99	12.95	2.52	2.74	12.40	0.23	5.74	10.16	2.44	0.18	0.28	99.63
SON0012-130-A2	50.04	12.88	2.50	2.53	12.49	0.23	5.60	10.10	2.51	0.18	0.30	99.36
SON0012-123-A	50.25	15.24	0.90	1.12	7.70	0.15	8.93	13.00	2.23	0.06	0.05	99.63
SON0012-108-A	50.20	13.14	2.22	2.37	11.86	0.22	6.27	10.58	2.35	0.14	0.20	99.55
ALV0735-004G	51.00	13.40	1.70	1.40	11.30	0.21	6.60	11.20	2.30	0.07	0.12	99.30
ALV0714-004G	51.40	13.50	1.72	1.30	11.30	0.18	6.60	11.00	2.30	0.10	0.12	99.52
ALV0994-001D	53.10	12.22	2.70	2.70	12.80	0.22	3.90	8.60	2.80	0.19	0.33	99.56
ALV1002-004B	54.30	12.00	2.60	2.60	12.91	0.24	3.50	8.20	3.00	0.20	0.47	100.02
ALV0994-003A	55.90	11.50	2.60	1.90	13.70	0.25	2.50	7.32	3.20	0.22	0.54	99.63
ALV0999-001B	56.30	11.10	2.00	1.20	15.10	0.24	1.60	6.80	3.00	0.25	0.72	98.31
12-40	49.63	15.51	1.02	1.12	8.97	0.19	8.79	12.03	2.15	0.05	0.09	99.55
D6-C44	57.35	13.33	1.80	2.23	10.07	0.20	2.67	7.14	3.33	0.56	0.18	98.86
714-G1	51.40	13.60	1.70	1.00	11.70	0.19	6.60	11.00	2.30	0.10	0.14	99.73
731-G4	51.00	13.40	1.70	1.90	11.00	0.22	6.50	11.20	2.30	0.08	0.12	99.42
	51.77	13.22		1.87	11.52		5.90	10.21	2.48	0.18		
	49.63	10.48		0.84	7.70		1.60	6.80	1.82	0.04		
	57.35	15.54		3.07	15.65		9.46	13.00	3.33	0.56		

MOLES	Si	Al	Ti	Fe3+	Fe2+	Mn	Mg	Ca	Na	K	P	SUM
	0.8322	0.1524	0.0110	0.0053	0.1114	0.0023	0.2347	0.2289	0.0294	0.0004	0.0007	1.6085
	0.8260	0.1521	0.0128	0.0073	0.1249	0.0027	0.2181	0.2144	0.0347	0.0005	0.0006	1.5941
	0.8433	0.1354	0.0225	0.0077	0.1567	0.0031	0.1752	0.1959	0.0376	0.0018	0.0012	1.5805
	0.8451	0.1326	0.0239	0.0117	0.1564	0.0038	0.1509	0.1948	0.0395	0.0021	0.0021	1.5631
	0.9355	0.1097	0.0305	0.0163	0.1841	0.0032	0.0643	0.1308	0.0463	0.0044	0.0036	1.5289
	0.8428	0.1183	0.0357	0.0169	0.1917	0.0037	0.1206	0.1726	0.0394	0.0024	0.0020	1.5459
	0.8503	0.1028	0.0464	0.0192	0.2178	0.0041	0.0896	0.1556	0.0408	0.0030	0.0032	1.5328
	0.8593	0.1198	0.0252	0.0142	0.1609	0.0032	0.1680	0.1932	0.0373	0.0016	0.0011	1.5838
	0.8307	0.1460	0.0163	0.0082	0.1333	0.0025	0.2079	0.2118	0.0355	0.0014	0.0007	1.5943
	0.8330	0.1409	0.0194	0.0101	0.1388	0.0027	0.2030	0.2032	0.0349	0.0019	0.0010	1.5888
	0.8320	0.1270	0.0315	0.0172	0.1726	0.0032	0.1424	0.1811	0.0394	0.0019	0.0020	1.5503
	0.8328	0.1263	0.0313	0.0158	0.1738	0.0032	0.1389	0.1800	0.0405	0.0019	0.0021	1.5469
	0.8363	0.1495	0.0113	0.0070	0.1072	0.0021	0.2216	0.2317	0.0360	0.0006	0.0004	1.6036
	0.8355	0.1289	0.0278	0.0148	0.1651	0.0031	0.1556	0.1886	0.0379	0.0015	0.0014	1.5601
	0.8488	0.1314	0.0213	0.0088	0.1573	0.0030	0.1638	0.1997	0.0371	0.0007	0.0008	1.5726
	0.8555	0.1324	0.0215	0.0081	0.1573	0.0025	0.1638	0.1961	0.0371	0.0011	0.0008	1.5762
	0.8838	0.1198	0.0338	0.0169	0.1782	0.0031	0.0968	0.1533	0.0452	0.0020	0.0023	1.5352
	0.9037	0.1177	0.0325	0.0163	0.1797	0.0034	0.0868	0.1462	0.0484	0.0021	0.0033	1.5402
	0.9304	0.1128	0.0325	0.0119	0.1907	0.0035	0.0620	0.1305	0.0516	0.0023	0.0038	1.5321
	0.9370	0.1089	0.0250	0.0075	0.2102	0.0034	0.0397	0.1212	0.0484	0.0027	0.0051	1.5090
	0.8260	0.1521	0.0128	0.0070	0.1249	0.0027	0.2181	0.2144	0.0347	0.0005	0.0006	1.5938
	0.9545	0.1307	0.0225	0.0140	0.1402	0.0028	0.0662	0.1273	0.0537	0.0059	0.0013	1.5192
	0.8555	0.1334	0.0213	0.0063	0.1629	0.0027	0.1638	0.1961	0.0371	0.0011	0.0010	1.5809
	0.8488	0.1314	0.0213	0.0119	0.1531	0.0031	0.1613	0.1997	0.0371	0.0008	0.0008	1.5693
	0.86161	0.12969		0.01169	0.16038		0.14637	0.18197	0.03998	0.00187	0.00175	1.56292
	0.826	0.10278		0.00526	0.10718		0.0397	0.12122	0.02936	0.00042	0.00035	1.50903
	0.95448	0.15241		0.01922	0.21783		0.23471	0.23174	0.05373	0.00595	0.00507	1.60855

MOLE	Si	Al	Ti	Fe3+	Fe2+	Mn	Mg	Ca	Na	K
FRACTION	0.51734	0.09475	0.00685	0.00327	0.06923	0.00140	0.14592	0.14229	0.01826	0.00026
	0.51817	0.09543	0.00801	0.00456	0.07832	0.00168	0.13681	0.13453	0.02176	0.00033
	0.53358	0.08570	0.01425	0.00487	0.09916	0.00196	0.11083	0.12396	0.02379	0.00114
	0.54069	0.08483	0.01529	0.00749	0.10009	0.00244	0.09651	0.12465	0.02529	0.00136
	0.61189	0.07178	0.01997	0.01069	0.12045	0.00212	0.04203	0.08558	0.03029	0.00285
	0.54518	0.07651	0.02307	0.01094	0.12398	0.00237	0.07800	0.11162	0.02547	0.00158
	0.55473	0.06706	0.03029	0.01254	0.14211	0.00267	0.05843	0.10153	0.02663	0.00194
	0.54256	0.07561	0.01588	0.00898	0.10160	0.00205	0.10606	0.12201	0.02353	0.00101
	0.52101	0.09160	0.01021	0.00515	0.08364	0.00159	0.13041	0.13283	0.02226	0.00087
	0.52427	0.08870	0.01221	0.00639	0.08734	0.00169	0.12774	0.12790	0.02193	0.00120
	0.53666	0.08192	0.02034	0.01107	0.11133	0.00209	0.09186	0.11682	0.02539	0.00123
	0.53839	0.08166	0.02023	0.01024	0.11239	0.00210	0.08982	0.11639	0.02618	0.00124
	0.52152	0.09321	0.00702	0.00437	0.06683	0.00132	0.13816	0.14451	0.02244	0.00040
	0.53552	0.08260	0.01781	0.00951	0.10581	0.00199	0.09971	0.12089	0.02430	0.00095
	0.53974	0.08357	0.01353	0.00557	0.10001	0.00188	0.10413	0.12696	0.02360	0.00047
	0.54273	0.08400	0.01366	0.00516	0.09979	0.00161	0.10389	0.12440	0.02354	0.00067
	0.57568	0.07807	0.02201	0.01101	0.11606	0.00202	0.06303	0.09986	0.02943	0.00131
	0.58675	0.07641	0.02113	0.01057	0.11670	0.00220	0.05638	0.09491	0.03143	0.00138
	0.60725	0.07362	0.02124	0.00777	0.12446	0.00230	0.04049	0.08517	0.03370	0.00152
	0.62094	0.07214	0.01659	0.00498	0.13928	0.00224	0.02631	0.08033	0.03208	0.00176
	0.51825	0.09544	0.00801	0.00440	0.07834	0.00168	0.13683	0.13455	0.02176	0.00033
	0.62830	0.08606	0.01483	0.00919	0.09226	0.00186	0.04361	0.08378	0.03537	0.00391
	0.54112	0.08437	0.01346	0.00396	0.10301	0.00169	0.10358	0.12403	0.02347	0.00067
	0.54087	0.08374	0.01356	0.00758	0.09756	0.00198	0.10276	0.12722	0.02365	0.00054

P	SUM	Mg#	Na+K	Ca/(Ca+Na)	CaO/Al2O3	FeO	Fe2O3	FACT	FeOT	Fe2O3/(FeO+Fe2O3)	FeOT	Fe2O3
0.00044	1.00000	0.6782	1.8600	0.8863	0.8263	8.00	0.84	0.8998	8.76	0.09	8.76	0.84
0.00040	1.00000	0.6359	2.2000	0.8608	0.7756	8.97	1.16	0.8998	10.01	0.10	10.01	1.16
0.00076	1.00000	0.5278	2.5000	0.8390	0.7958	11.26	1.23	0.8998	12.37	0.09	12.37	1.23
0.00135	1.00000	0.4909	2.6500	0.8313	0.8084	11.24	1.87	0.8998	12.92	0.13	12.92	1.87
0.00235	1.00000	0.2587	3.2800	0.7386	0.6559	13.23	2.61	0.8998	15.58	0.14	15.58	2.61
0.00128	1.00000	0.3862	2.6700	0.8142	0.8027	13.77	2.70	0.8998	16.20	0.14	16.20	2.70
0.00207	1.00000	0.2914	2.8100	0.7922	0.8330	15.65	3.07	0.8998	18.41	0.14	18.41	3.07
0.00071	1.00000	0.5107	2.4600	0.8383	0.8878	11.56	2.27	0.8998	13.60	0.14	13.60	2.27
0.00044	1.00000	0.6093	2.3300	0.8564	0.7979	9.58	1.31	0.8998	10.76	0.11	10.76	1.31
0.00062	1.00000	0.5939	2.3400	0.8536	0.7933	9.97	1.62	0.8998	11.43	0.12	11.43	1.62
0.00127	1.00000	0.4521	2.6200	0.8214	0.7846	12.40	2.74	0.8998	14.87	0.16	14.87	2.74
0.00137	1.00000	0.4442	2.6900	0.8164	0.7842	12.49	2.53	0.8998	14.77	0.15	14.77	2.53
0.00022	1.00000	0.6740	2.2900	0.8656	0.8530	7.70	1.12	0.8998	8.71	0.11	8.71	1.12
0.00090	1.00000	0.4852	2.4900	0.8326	0.8052	11.86	2.37	0.8998	13.99	0.14	13.99	2.37
0.00054	1.00000	0.5101	2.3700	0.8433	0.8358	11.30	1.40	0.8998	12.56	0.10	12.56	1.40
0.00054	1.00000	0.5101	2.4000	0.8409	0.8148	11.30	1.30	0.8998	12.47	0.09	12.47	1.30
0.00151	1.00000	0.3520	2.9900	0.7724	0.7038	12.80	2.70	0.8998	15.23	0.15	15.23	2.70
0.00215	1.00000	0.3258	3.2000	0.7512	0.6833	12.91	2.60	0.8998	15.25	0.15	15.25	2.60
0.00248	1.00000	0.2454	3.4200	0.7165	0.6365	13.70	1.90	0.8998	15.41	0.11	15.41	1.90
0.00336	1.00000	0.1589	3.2500	0.7146	0.6126	15.10	1.20	0.8998	16.18	0.07	16.18	1.20
0.00040	1.00000	0.6359	2.2000	0.8608	0.7756	8.97	1.12	0.8998	9.98	0.10	9.98	1.12
0.00083	1.00000	0.3209	3.8900	0.7032	0.5356	10.07	2.23	0.8998	12.08	0.16	12.08	2.23
0.00062	1.00000	0.5014	2.4000	0.8409	0.8088	11.70	1.00	0.8998	12.60	0.07	12.60	1.00
0.00054	1.00000	0.5130	2.3800	0.8433	0.8358	11.00	1.90	0.8998	12.71	0.13	12.71	1.90
	Ave	0.4630	2.6538				1.87					1.87
	Min	0.1589	1.8600				0.84					0.84
	Max	0.6782	3.8900				3.07					3.07

FeO	Fe2O3/(FeO+Fe2O3)	FeOT CALC	XFeT	TC	TK	P b	P Kb	DIXIKil	DIXIKRESS	E TERM	F TERM
8.00	0.0950	8.7558	0.0758	1200	1473.15	1.0	0.0010	0.4826	0.2130	0.028379	-0.000048
8.97	0.1145	10.0138	0.0874	1200	1473.15	1.0	0.0010	0.5064	0.1862	0.028379	-0.000048
11.26	0.0985	12.3668	0.1089	1200	1473.15	1.0	0.0010	0.5550	0.1518	0.028379	-0.000048
11.24	0.1426	12.9226	0.1151	1200	1473.15	1.0	0.0010	0.5833	0.1549	0.028379	-0.000048
13.23	0.1648	15.5785	0.1418	1200	1473.15	1.0	0.0010	0.5947	0.0487	0.028379	-0.000048
13.77	0.1639	16.1995	0.1459	1200	1473.15	1.0	0.0010	0.6147	0.0780	0.028379	-0.000048
15.65	0.1640	18.4124	0.1672	1200	1473.15	1.0	0.0010	0.6523	0.0369	0.028379	-0.000048
11.56	0.1641	13.6026	0.1195	1200	1473.15	1.0	0.0010	0.5849	0.1464	0.028379	-0.000048
9.58	0.1203	10.7587	0.0939	1200	1473.15	1.0	0.0010	0.5294	0.1838	0.028379	-0.000048
9.97	0.1398	11.4277	0.1001	1200	1473.15	1.0	0.0010	0.5313	0.1633	0.028379	-0.000048
12.40	0.1810	14.8655	0.1335	1200	1473.15	1.0	0.0010	0.5948	0.1025	0.028379	-0.000048
12.49	0.1684	14.7665	0.1329	1200	1473.15	1.0	0.0010	0.5998	0.1074	0.028379	-0.000048
7.70	0.1270	8.7078	0.0756	1200	1473.15	1.0	0.0010	0.5288	0.2492	0.028379	-0.000048
11.86	0.1665	13.9925	0.1248	1200	1473.15	1.0	0.0010	0.5801	0.1217	0.028379	-0.000048
11.30	0.1102	12.5597	0.1112	1200	1473.15	1.0	0.0010	0.5641	0.1568	0.028379	-0.000048
11.30	0.1032	12.4698	0.1101	1200	1473.15	1.0	0.0010	0.5554	0.1505	0.028379	-0.000048
12.80	0.1742	15.2295	0.1381	1200	1473.15	1.0	0.0010	0.5951	0.0726	0.028379	-0.000048
12.91	0.1676	15.2525	0.1378	1200	1473.15	1.0	0.0010	0.6012	0.0730	0.028379	-0.000048
13.70	0.1218	15.4096	0.1400	1200	1473.15	1.0	0.0010	0.6026	0.0583	0.028379	-0.000048
15.10	0.0736	16.1798	0.1492	1200	1473.15	1.0	0.0010	0.5944	0.0212	0.028379	-0.000048
8.97	0.1110	9.9778	0.0871	1200	1473.15	1.0	0.0010	0.5060	0.1868	0.028379	-0.000048
10.07	0.1813	12.0766	0.1106	1200	1473.15	1.0	0.0010	0.5620	0.1043	0.028379	-0.000048
11.70	0.0787	12.5998	0.1109	1200	1473.15	1.0	0.0010	0.5542	0.1466	0.028379	-0.000048
11.00	0.1473	12.7096	0.1127	1200	1473.15	1.0	0.0010	0.5680	0.1551	0.028379	-0.000048
11.52	0.1366										
7.70	0.0736										
15.65	0.1813										

G TERM	H TERM	KdKilinc	LnfO2Kil	LnfO2Kress	logfO2Kil	logfO2Kress	FMQ	NNO	DFMQKIL	DFMQKress	DNNOKIL	DNNOKress
0.000002	0.000000	0.0472	-21.0332	-22.5499	-9.1346	-9.7933	-8.3008	-7.5629	-0.8338	-1.4925	-1.5717	-2.2304
0.000002	0.000000	0.0582	-20.1886	-21.3505	-8.7678	-9.2724	-8.3008	-7.5629	-0.4670	-0.9716	-1.2049	-1.7095
0.000002	0.000000	0.0491	-21.1834	-22.0361	-9.1998	-9.5702	-8.3008	-7.5629	-0.8990	-1.2694	-1.6369	-2.0072
0.000002	0.000000	0.0749	-19.3874	-19.9052	-8.4199	-8.6447	-8.3008	-7.5629	-0.1191	-0.3439	-0.8569	-1.0818
0.000002	0.000000	0.0888	-18.6597	-18.4941	-8.1038	-8.0319	-8.3008	-7.5629	0.1970	0.2689	-0.5409	-0.4689
0.000002	0.000000	0.0882	-18.7791	-18.6746	-8.1557	-8.1103	-8.3008	-7.5629	0.1451	0.1905	-0.5927	-0.5474
0.000002	0.000000	0.0883	-18.9493	-18.4628	-8.2296	-8.0183	-8.3008	-7.5629	0.0712	0.2825	-0.6667	-0.4554
0.000002	0.000000	0.0883	-18.6361	-19.0165	-8.0935	-8.2588	-8.3008	-7.5629	0.2073	0.0420	-0.5306	-0.6958
0.000002	0.000000	0.0615	-20.0382	-21.0532	-8.7025	-9.1433	-8.3008	-7.5629	-0.4017	-0.8425	-1.1395	-1.5804
0.000002	0.000000	0.0731	-19.2576	-20.0689	-8.3635	-8.7158	-8.3008	-7.5629	-0.0627	-0.4150	-0.8006	-1.1529
0.000002	0.000000	0.0994	-18.1413	-18.1903	-7.8787	-7.9000	-8.3008	-7.5629	0.4222	0.4009	-0.3157	-0.3370
0.000002	0.000000	0.0911	-18.5624	-18.6591	-8.0615	-8.1035	-8.3008	-7.5629	0.2393	0.1973	-0.4986	-0.5406
0.000002	0.000000	0.0654	-19.7532	-21.0718	-8.5787	-9.1514	-8.3008	-7.5629	-0.2779	-0.8506	-1.0158	-1.5885
0.000002	0.000000	0.0899	-18.5340	-18.8009	-8.0492	-8.1651	-8.3008	-7.5629	0.2516	0.1357	-0.4863	-0.6022
0.000002	0.000000	0.0557	-20.6489	-21.4192	-8.9677	-9.3022	-8.3008	-7.5629	-0.6669	-1.0014	-1.4048	-1.7393
0.000002	0.000000	0.0518	-20.9484	-21.7652	-9.0978	-9.4525	-8.3008	-7.5629	-0.7970	-1.1517	-1.5349	-1.8896
0.000002	0.000000	0.0949	-18.3554	-18.2744	-7.9717	-7.9365	-8.3008	-7.5629	0.3291	0.3643	-0.4087	-0.3736
0.000002	0.000000	0.0906	-18.5963	-18.5139	-8.0763	-8.0405	-8.3008	-7.5629	0.2245	0.2603	-0.5134	-0.4775
0.000002	0.000000	0.0624	-20.3087	-20.3414	-8.8199	-8.8341	-8.3008	-7.5629	-0.5191	-0.5333	-1.2570	-1.2712
0.000002	0.000000	0.0358	-22.8199	-22.9929	-9.9106	-9.9857	-8.3008	-7.5629	-1.6098	-1.6849	-2.3476	-2.4228
0.000002	0.000000	0.0562	-20.3473	-21.5326	-8.8367	-9.3515	-8.3008	-7.5629	-0.5359	-1.0507	-1.2738	-1.7886
0.000002	0.000000	0.0996	-17.9814	-18.1879	-7.8092	-7.8989	-8.3008	-7.5629	0.4916	0.4019	-0.2463	-0.3360
0.000002	0.000000	0.0385	-22.3026	-23.2612	-9.6859	-10.1022	-8.3008	-7.5629	-1.3851	-1.8014	-2.1230	-2.5393
0.000002	0.000000	0.0777	-19.1459	-19.7153	-8.3150	-8.5622	-8.3008	-7.5629	-0.0142	-0.2614	-0.7521	-0.9993
	Ave	0.0996	-17.9814	-18.1879	-7.8092	-7.8989			-0.2504	-0.4636	-0.9883	-1.2015
	Min	0.0358	-22.8199	-23.2612	-9.9106	-10.1022			-1.6098	-1.8014	-2.3476	-2.5393
	Max	0.0719	-19.6899	-20.1808	-8.5512	-8.7644			0.4916	0.4019	-0.2463	-0.3360

Ridge Data: Olivine-Liquid

		TK	SiO2	Al2O3	TiO2	FeO	MnO	MgO	CaO	Na2O	K2O	P2O5	TOTAL
TR-1D2	Galap1	1184	50.07	12.8	2.18	14.23	0.23	5.83	10.21	2.79	0.15		98.490
TR-3D1	Galap2	1205	50.32	14.05	1.46	11.49	0.17	7.27	11.49	2.3	0.1	0	98.650
TR-25D1	Galap3	1187	50.3	14.25	1.71	11.05	0.2	7.15	11.53	2.59	0.23	0	99.010
CTW-10D1	Galap4	1207	49.84	13.96	1.58	11.09	0.19	6.9	11.85	2.52	0.22	0	98.150
TR-12D1	Galap5	1207	50.25	14.42	1.25	10.2	0.19	7.74	12.05	2.42	0.14	0	98.660
TR-23D2	Galap6	1187	50.35	13.92	1.64	11.63	0.2	6.7	10.78	2.68	0.2	0	98.100
TR-15D1	Galap7	1186	50.62	14.35	1.33	10.65	0.2	7.5	12.17	2.37	0.1	0	99.290
TR-16D1	Galap8	1190	50.73	14.03	1.62	11.9	0.21	6.91	11.06	2.51	0.16	0	99.130
DS-D8A	Galap9	1211	49.83	14.09	1.55	11.42	0.2	7.74	10.96	2.38	0.13	0	98.300
DS-D7A	Galap10	1225	49.64	15.18	1.08	9.23	0.14	8.69	12.22	2.31	0.09	0	98.580
DS-D5	Galap11	1229	49.37	15.86	1.03	8.87	0.11	8.91	12.32	2.31	0.07	0	98.850
TR-6D1	Galap12	1203	49.33	14.59	2.15	10.37	0.16	6.29	10.61	3.1	0.69	0	97.290
TR-6D2	Galap13	1203	49.44	14.16	1.51	11.3	0.2	7.47	11.73	2.59	0.12	0	98.520
TR-7D2	Galap14	1196	49.32	14.15	1.56	11.42	0.18	7.19	11.9	2.75	0.15	0	98.620
TR-8D1	Galap15	1148	49.62	13.16	2.52	14.18	0.2	5.11	9.59	3.39	0.34	0	98.110
TR-9D1	Galap16	1199	47.91	16.41	1.92	9.75	0.14	7.48	11.46	3.07	0.38	0	98.520
TR-9D3	Galap17	1187	48.26	16.36	1.9	9.89	0.2	7.82	11.28	2.97	0.35	0	99.030

Mg#	Na+K	Ca/(Ca+Na)	CaO/Al2O3	AVE MPH*	Kd*	**NORM**	SiO2	Al2O3	TiO2	Fe2O3	FeO
0.4221	2.9400	0.8017	0.7977	0.7100	0.2983		50.775	12.980	2.211	1.2227	13.330
0.5300	2.4000	0.8466	0.8178	0.7900	0.2998		50.959	14.228	1.479	0.9717	10.762
0.5356	2.8200	0.8310	0.8091	0.8050	0.2794		50.719	14.369	1.724	1.6395	9.667
0.5259	2.7400	0.8386	0.8489	0.8000	0.2773		50.691	14.198	1.607	1.7445	9.710
0.5749	2.5600	0.8462	0.8356	0.8300	0.2770		50.850	14.592	1.265	1.6164	8.867
0.5066	2.8800	0.8163	0.7744	0.7900	0.2730		51.219	14.160	1.668	2.0614	9.976
0.5566	2.4700	0.8502	0.8481	0.8200	0.2756		50.891	14.427	1.337	1.7807	9.105
0.5086	2.6700	0.8296	0.7883	0.7900	0.2751		51.084	14.128	1.631	1.7807	10.381
0.5471	2.5100	0.8357	0.7779	0.8100	0.2834		50.612	14.311	1.574	1.5661	10.190
0.6266	2.4000	0.8539	0.8050	0.8500	0.2962		50.315	15.387	1.095	0.7843	8.650
0.6417	2.3800	0.8549	0.7768	0.8600	0.2915		49.901	16.031	1.041	0.8645	8.188
0.5195	3.7900	0.7909	0.7272	0.8000	0.2703		50.615	14.970	2.206	1.7480	9.067
0.5409	2.7100	0.8334	0.8284	0.8100	0.2764		50.096	14.348	1.530	1.7319	9.891
0.5288	2.9000	0.8270	0.8410	0.8000	0.2806		49.934	14.326	1.579	1.5252	10.190
0.3911	3.7300	0.7576	0.7287	0.7000	0.2753		50.463	13.384	2.563	2.2188	12.425
0.5776	3.4500	0.8049	0.6984	0.8350	0.2702		48.560	16.632	1.946	1.4402	8.586
0.5850	3.3200	0.8076	0.6895	0.8400	0.2685		48.656	16.494	1.916	1.5621	8.566
						Ave	50.373	14.645		1.545	9.856
						Min	48.560	12.980		0.784	8.188
						Max	51.219	16.632		2.219	13.330

MnO	MgO	CaO	Na2O	K2O	P2O5	TOTAL	Mg#	Na+K	Ca/(Ca+Na)	CaO/Al2O3	Kd
0.233	5.912	10.354	2.829	0.152	0.000	100.00	0.4415	2.9814	0.8017	0.7977	0.3229
0.172	7.362	11.636	2.329	0.101	0.000	100.00	0.5494	2.4305	0.8466	0.8178	0.3242
0.202	7.210	11.626	2.612	0.232	0.000	100.00	0.5707	2.8435	0.8310	0.8091	0.3220
0.193	7.018	12.052	2.563	0.224	0.000	100.00	0.5630	2.7868	0.8386	0.8489	0.3221
0.192	7.832	12.194	2.449	0.142	0.000	100.00	0.6116	2.5906	0.8462	0.8356	0.3225
0.203	6.816	10.966	2.726	0.203	0.000	100.00	0.5491	2.9297	0.8163	0.7744	0.3237
0.201	7.540	12.235	2.383	0.101	0.000	100.00	0.5962	2.4832	0.8502	0.8481	0.3241
0.211	6.958	11.137	2.528	0.161	0.000	100.00	0.5444	2.6886	0.8296	0.7883	0.3176
0.203	7.861	11.132	2.417	0.132	0.000	100.00	0.5790	2.5494	0.8357	0.7779	0.3226
0.142	8.808	12.386	2.341	0.091	0.000	100.00	0.6448	2.4327	0.8539	0.8050	0.3203
0.111	9.006	12.453	2.335	0.071	0.000	100.00	0.6622	2.4056	0.8549	0.7768	0.3192
0.164	6.454	10.886	3.181	0.708	0.000	100.00	0.5592	3.8887	0.7909	0.7272	0.3172
0.203	7.569	11.886	2.624	0.122	0.000	100.00	0.5770	2.7459	0.8334	0.8284	0.3200
0.182	7.279	12.048	2.784	0.152	0.000	100.00	0.5601	2.9361	0.8270	0.8410	0.3184
0.203	5.197	9.753	3.448	0.346	0.000	100.00	0.4271	3.7934	0.7576	0.7287	0.3195
0.142	7.581	11.615	3.112	0.385	0.000	100.00	0.6115	3.4968	0.8049	0.6984	0.3110
0.202	7.884	11.373	2.994	0.353	0.000	100.00	0.6213	3.3473	0.8076	0.6895	0.3125
	7.311	11.514	2.686	0.216		**Ave**	0.5687	2.9018			0.3200
	5.197	9.753	2.329	0.071		**Min**	0.4271	2.4056			0.3110
	9.006	12.453	3.448	0.708		**Max**	0.6622	3.8887			0.3242

Fe2O3/(FeO+Fe2O3)	TK	P b	LnfO2Kil	LnfO2Kress	logfO2Kil	logfO2Kress	FMQ	NNO
0.0840	1457.2	1.0	-22.7007	-23.3143	-9.8588	-10.1253	-8.4879	-7.9011
0.0828	1478.2	1.0	-21.9076	-22.9928	-9.5143	-9.9856	-8.2432	-7.6617
0.1450		1.0	-19.4645	-20.2670	-8.4533	-8.8019	-8.3821	-7.7976
0.1523	1480.2	1.0	-18.8900	-19.6353	-8.2038	-8.5275	-8.2202	-7.6392
0.1542	1480.2	1.0	-18.6763	-19.5792	-8.1110	-8.5031	-8.2202	-7.6392
0.1713	1460.2	1.0	-18.7275	-19.3038	-8.1333	-8.3835	-8.4525	-7.8665
0.1636	1459.2	1.0	-18.9264	-19.7855	-8.2196	-8.5927	-8.4643	-7.8780
0.1464	1463.2	1.0	-19.4387	-20.1157	-8.4421	-8.7361	-8.4172	-7.8320
0.1332	1484.2	1.0	-19.2777	-20.0490	-8.3722	-8.7072	-8.1745	-7.5945
0.0831	1498.2	1.0	-21.2443	-22.6460	-9.2263	-9.8350	-8.0165	-7.4399
0.0955	1502.2	1.0	-20.3844	-21.7533	-8.8528	-9.4473	-7.9719	-7.3962
0.1616	1445.2	1.0	-19.6622	-20.3800	-8.5392	-8.8509	-8.6309	-8.0410
0.1490	1476.2	1.0	-19.0778	-19.8198	-8.2854	-8.6076	-8.2662	-7.6842
0.1302	1469.2	1.0	-20.0892	-20.8981	-8.7246	-9.0759	-8.3472	-7.7634
0.1515	1421.2	1.0	-20.8812	-21.1058	-9.0686	-9.1661	-8.9241	-8.3280
0.1436	1472.2	1.0	-19.3872	-20.2832	-8.4198	-8.8089	-8.3124	-7.7294
0.1542	1481.2	1.0	-18.6831	-19.5142	-8.1140	-8.4749	-8.2088	-7.6280

0.1354	
0.0828	
0.1713	

	DFMQKIL	DFMQKress	DNNOKIL	DNNOKress
	-1.3709	-1.6374	-1.9577	-2.2242
	-1.2712	-1.7425	-1.8527	-2.3240
	-0.0712	-0.4197	-0.6557	-1.0042
	0.0164	-0.3072	-0.5646	-0.8883
	0.1092	-0.2829	-0.4718	-0.8639
	0.3192	0.0689	-0.2668	-0.5171
	0.2446	-0.1285	-0.3416	-0.7147
	-0.0249	-0.3189	-0.6101	-0.9042
	-0.1977	-0.5326	-0.7777	-1.1127
	-1.2098	-1.8185	-1.7864	-2.3951
	-0.8809	-1.4754	-1.4566	-2.0511
	0.0917	-0.2201	-0.4982	-0.8099
	-0.0192	-0.3415	-0.6012	-0.9235
	-0.3774	-0.7287	-0.9612	-1.3125
	-0.1444	-0.2420	-0.7406	-0.8382
	-0.1074	-0.4965	-0.6904	-1.0795
	0.0948	-0.2661	-0.4859	-0.8469
Ave	-0.2823	**-0.6406**	-0.8658	-1.2241
Min	-1.3709	**-1.8185**	-1.9577	-2.3951
Max	0.3192	**0.0689**	-0.2668	-0.5171

Islands Data: Olivine-Liquid

		TK	SiO2	Al2O3	TiO2	FeO	MnO	MgO	CaO	Na2O	K2O	P2O5	TOTAL
D-01	Darwin1	1175	47.58	12.49	3.67	13.69	0.22	7.26	10.57	3.17	0.45	0.26	99.36
D-100	Darwin2	1175	47.26	12.75	3.69	13.78	0.21	7.26	10.45	3.27	0.51	0.38	99.56
F WR	Fern1	1150	48.92	15.6	3.35	11.16	0.17	5.57	11.43	2.95	0.51	0.34	100.00
M WR	Fern2	1150	48.99	16.41	2.59	9.82	0.16	6.59	12.40	2.44	0.35	0.25	100.00
I WR	Fern3	1150	48.52	16.72	3.15	10.48	0.17	5.36	11.88	2.93	0.48	0.31	100.00
1825 WR	Fern4	1150	48.61	15.96	3.27	11.35	0.18	5.82	11.17	2.94	0.58	0.12	100.00
58b WR	Fern5	1150	48.46	14.19	2.54	11.94	0.19	6.09	10.90	2.97	0.54	0.36	98.18
61a WR	Fern6	1150	48.70	16.58	3.08	10.57	0.17	5.58	11.61	2.91	0.47	0.32	100.00
61b WR	Fern7	1150	48.49	16.50	3.13	10.77	0.17	5.55	11.72	2.85	0.48	0.32	100.00
68a WR	Fern8	1150	48.73	17.78	2.81	9.86	0.15	5.23	11.90	2.81	0.44	0.28	100.00
72 WR	Fern9	1150	48.71	17.43	2.85	9.69	0.16	5.49	12.06	2.81	0.47	0.31	100.00
72 WR	Fern10	1150	48.78	17.36	3.04	9.43	0.18	5.72	11.93	2.84	0.52	0.20	100.00
77a WR	Fern11	1150	48.74	15.72	3.32	10.89	0.18	5.61	11.65	3.00	0.53	0.35	100.00
77c WR	Fern12	1150	48.91	16.09	3.26	10.60	0.17	5.41	11.74	2.94	0.54	0.34	100.00
84a WR	Fern13	1150	48.83	14.16	3.72	12.05	0.19	6.05	10.99	3.03	0.59	0.38	100.00
84c WR	Fern14	1150	48.45	14.86	3.60	11.75	0.19	5.59	11.57	3.05	0.57	0.37	100.00
84d WR	Fern15	1150	48.82	14.77	3.56	11.62	0.18	5.89	11.31	2.94	0.55	0.35	100.00
84e WR	Fern16	1150	47.37	14.61	3.46	11.23	0.18	5.57	11.02	2.87	0.55	0.36	97.21
88d WR	Fern17	1150	48.79	15.40	3.50	11.23	0.18	5.41	11.64	2.96	0.54	0.35	100.00
R9519	Rocared1	1150	49.54	17.26	3.30	9.37	0.13	4.90	10.25	3.83	0.94	0.54	100.07
R9519	Rocared2	1150	49.54	17.26	3.30	9.37	0.13	4.90	10.25	3.83	0.94	0.54	100.07
R958	Rocared3	1150	48.18	16.43	3.01	10.66	0.13	5.93	9.48	3.63	0.89	0.43	98.77
R958	Rocared4	1150	48.18	16.43	3.01	10.66	0.13	5.93	9.48	3.63	0.89	0.43	98.77
R9520b	Rocared5	1150	47.35	15.25	2.79	11.45	0.17	8.87	9.47	3.49	0.75	0.42	100.00
R9511	Rocared6	1150	47.61	15.77	2.91	10.56	0.16	8.43	9.78	3.59	0.73	0.47	100.00
						10.96							
						9.37							
						13.78							

Mg#	Na+K	Ca/(Ca+Na)	CaO/Al2O3	AVE MPH	Kd	**NORM**	SiO2	Al2O3	TiO2	Fe2O3	FeO
0.4860	3.6200	0.7865	0.8463	0.7800	0.2667		47.783	12.543	3.686	2.1704	11.794
0.4843	3.7800	0.7793	0.8196	0.7800	0.2649		47.365	12.778	3.698	2.1721	11.857
0.4708	3.4600	0.8106	0.7327	0.7600	0.2810		48.849	15.577	3.345	1.4471	9.842
0.5447	2.7936	0.8486	0.7553	0.8100	0.2806		48.926	16.389	2.590	1.3476	8.591
0.4767	3.4031	0.8176	0.7104	0.7600	0.2876		48.471	16.704	3.147	1.0721	9.506
0.4776	3.5218	0.8076	0.6995	0.7700	0.2731		48.528	15.936	3.265	1.7329	9.766
0.4762	3.5100	0.8022	0.7681	0.7600	0.2871		49.297	14.435	2.584	1.2330	11.037
0.4848	3.3849	0.8149	0.7007	0.7700	0.2811		48.639	16.555	3.074	1.3466	9.344
0.4788	3.3357	0.8196	0.7104	0.7700	0.2744		48.408	16.477	3.125	1.6303	9.290
0.4859	3.2507	0.8236	0.6691	0.7700	0.2823		48.671	17.758	2.811	1.2534	8.723
0.5025	3.2869	0.8257	0.6919	0.7900	0.2684		48.627	17.404	2.849	1.6976	8.147
0.5193	3.3630	0.8224	0.6868	0.7950	0.2786		48.712	17.341	3.034	1.2902	8.259
0.4787	3.5287	0.8111	0.7409	0.7700	0.2743		48.663	15.695	3.319	1.6345	9.405
0.4766	3.4722	0.8154	0.7296	0.7600	0.2876		48.860	16.076	3.252	1.1202	9.576
0.4724	3.6197	0.8002	0.7759	0.7600	0.2827		48.761	14.144	3.716	1.4249	10.753
0.4589	3.6177	0.8074	0.7780	0.7500	0.2827		48.380	14.845	3.592	1.3501	10.521
0.4746	3.4968	0.8093	0.7654	0.7600	0.2853		48.759	14.755	3.554	1.2936	10.441
0.4689	3.4176	0.8094	0.7548	0.7600	0.2788		48.651	15.003	3.552	1.5097	10.181
0.4619	3.5061	0.8128	0.7560	0.7500	0.2861		48.731	15.379	3.492	1.2297	10.110
0.4824	4.7743	0.7472	0.5938	0.7750	0.2705		49.432	17.225	3.293	1.4195	8.078
0.4824	4.7743	0.7472	0.5938	0.7700	0.2783		49.446	17.230	3.294	1.1504	8.322
0.4978	4.5284	0.7423	0.5769	0.7850	0.2715		48.711	16.607	3.045	1.4732	9.446
0.4978	4.5284	0.7423	0.5769	0.7900	0.2635		48.696	16.601	3.044	1.7946	9.154
0.5801	4.2383	0.7498	0.6211	0.8350	0.2730		47.292	15.229	2.782	1.2103	10.347
0.5870	4.3166	0.7508	0.6203	0.8350	0.2809		47.567	15.754	2.905	0.8468	9.793
						Ave	48.569	15.778	3.202	1.434	9.691
						Min	47.292	12.543	2.584	0.847	8.078
						Max	49.446	17.758	3.716	2.172	11.857

MnO	MgO	CaO	Na2O	K2O	P2O5	TOTAL	Mg#	Na+K	Ca/(Ca+Na)	CaO/Al2O3	Kd
0.221	7.291	10.615	3.184	0.452	0.261	100.00	0.5242	3.6354	0.7865	0.8463	0.3108
0.210	7.276	10.473	3.277	0.511	0.381	100.00	0.5224	3.7884	0.7793	0.8196	0.3085
0.170	5.562	11.413	2.946	0.509	0.340	100.00	0.5018	3.4550	0.8106	0.7327	0.3181
0.159	6.579	12.378	2.440	0.350	0.250	100.00	0.5772	2.7898	0.8486	0.7553	0.3202
0.170	5.351	11.866	2.924	0.476	0.314	100.00	0.5008	3.3995	0.8176	0.7104	0.3168
0.179	5.809	11.147	2.935	0.581	0.120	100.00	0.5146	3.5157	0.8076	0.6995	0.3167
0.193	6.195	11.088	3.021	0.549	0.366	100.00	0.5001	3.5706	0.8022	0.7681	0.3160
0.172	5.573	11.599	2.911	0.470	0.317	100.00	0.5153	3.3804	0.8149	0.7007	0.3176
0.173	5.543	11.705	2.847	0.483	0.319	100.00	0.5154	3.3303	0.8196	0.7104	0.3177
0.153	5.222	11.882	2.811	0.436	0.280	100.00	0.5162	3.2466	0.8236	0.6691	0.3188
0.162	5.481	12.041	2.808	0.473	0.309	100.00	0.5453	3.2813	0.8257	0.6919	0.3188
0.181	5.710	11.910	2.841	0.518	0.203	100.00	0.5521	3.3587	0.8224	0.6868	0.3178
0.182	5.603	11.628	2.992	0.531	0.347	100.00	0.5150	3.5229	0.8111	0.7409	0.3172
0.173	5.406	11.729	2.933	0.535	0.340	100.00	0.5016	3.4683	0.8154	0.7296	0.3178
0.192	6.045	10.975	3.027	0.587	0.375	100.00	0.5005	3.6146	0.8002	0.7759	0.3164
0.195	5.583	11.549	3.043	0.569	0.373	100.00	0.4861	3.6128	0.8074	0.7780	0.3153
0.184	5.882	11.294	2.941	0.551	0.347	100.00	0.5010	3.4922	0.8093	0.7654	0.3171
0.187	5.716	11.324	2.946	0.564	0.366	100.00	0.5002	3.5103	0.8094	0.7548	0.3160
0.182	5.401	11.627	2.959	0.543	0.348	100.00	0.4878	3.5018	0.8128	0.7560	0.3174
0.130	4.890	10.228	3.823	0.941	0.540	100.00	0.5190	4.7642	0.7472	0.5938	0.3133
0.130	4.892	10.231	3.824	0.941	0.541	100.00	0.5117	4.7655	0.7472	0.5938	0.3130
0.131	5.990	9.581	3.675	0.903	0.436	100.00	0.5306	4.5780	0.7423	0.5769	0.3096
0.131	5.988	9.578	3.673	0.903	0.436	100.00	0.5383	4.5765	0.7423	0.5769	0.3100
0.169	8.864	9.459	3.487	0.746	0.415	100.00	0.6043	4.2331	0.7498	0.6211	0.3017
0.159	8.418	9.772	3.584	0.729	0.472	100.00	0.6051	4.3128	0.7508	0.6203	0.3028
Ave	6.011	11.084	3.114	0.594							
Min	4.890	9.459	2.440	0.350							
Max	8.864	12.378	3.824	0.941							

Fe2O3/(FeO+Fe2O3)	TK	Pb	LnfO2Kil	LnfO2Kress	logfO2Kil	logfO2Kress	FMQ	NNO
0.1554	1448.15	1.0	-20.0183	-20.3373	-8.6938	-8.8324	-8.5949	-8.0058
0.1548	1448.15	1.0	-20.0682	-20.3559	-8.7155	-8.8405	-8.5949	-8.0058
0.1282	1423.15	1.0	-21.4734	-22.3426	-9.3258	-9.7033	-8.8993	-8.3037
0.1356	1423.15	1.0	-20.9172	-22.0455	-9.0842	-9.5743	-8.8993	-8.3037
0.1014	1423.15	1.0	-22.6280	-23.7435	-9.8272	-10.3117	-8.8993	-8.3037
0.1507	1423.15	1.0	-20.5800	-21.3059	-8.9378	-9.2530	-8.8993	-8.3037
0.1005	1423.15	1.0	-22.8339	-23.7047	-9.9166	-10.2948	-8.8993	-8.3037
0.1260	1423.15	1.0	-21.4720	-22.4408	-9.3252	-9.7459	-8.8993	-8.3037
0.1493	1423.15	1.0	-20.5879	-21.4294	-8.9412	-9.3067	-8.8993	-8.3037
0.1256	1423.15	1.0	-21.3667	-22.4467	-9.2794	-9.7485	-8.8993	-8.3037
0.1724	1423.15	1.0	-19.7110	-20.6277	-8.5604	-8.9585	-8.8993	-8.3037
0.1351	1423.15	1.0	-21.0131	-22.1139	-9.1259	-9.6039	-8.8993	-8.3037
0.1481	1423.15	1.0	-20.7443	-21.5639	-9.0091	-9.3651	-8.8993	-8.3037
0.1047	1423.15	1.0	-22.5036	-23.5807	-9.7732	-10.2410	-8.8993	-8.3037
0.1170	1423.15	1.0	-22.0706	-22.8564	-9.5852	-9.9264	-8.8993	-8.3037
0.1137	1423.15	1.0	-22.2546	-23.1074	-9.6650	-10.0354	-8.8993	-8.3037
0.1102	1423.15	1.0	-22.3188	-23.2171	-9.6929	-10.0831	-8.8993	-8.3037
0.1291	1423.15	1.0	-21.4961	-22.3017	-9.3356	-9.6855	-8.8993	-8.3037
0.1084	1423.15	1.0	-22.4060	-23.3694	-9.7308	-10.1492	-8.8993	-8.3037
0.1495	1423.15	1.0	-20.7669	-21.6220	-9.0190	-9.3903	-8.8993	-8.3037
0.1214	1423.15	1.0	-21.8623	-22.8453	-9.4947	-9.9216	-8.8993	-8.3037
0.1349	1423.15	1.0	-21.2520	-21.9717	-9.2296	-9.5422	-8.8993	-8.3037
0.1639	1423.15	1.0	-20.2087	-20.8059	-8.7765	-9.0359	-8.8993	-8.3037
0.1047	1423.15	1.0	-22.4952	-23.3464	-9.7695	-10.1392	-8.8993	-8.3037
0.0796	1423.15	1.0	-23.8751	-25.0084	-10.3688	-10.8610	-8.8993	-8.3037
0.1288								
0.080								
0.172								

	DFMQKIL	DFMQKress	DNNOKIL	DNNOKress
	-0.0989	-0.2375	-0.6880	-0.8266
	-0.1206	-0.2456	-0.7097	-0.8347
	-0.4264	-0.8039	-1.0221	-1.3996
	-0.1849	-0.6749	-0.7805	-1.2706
	-0.9279	-1.4123	-1.5235	-2.0080
	-0.0385	-0.3537	-0.6341	-0.9493
	-1.0173	-1.3955	-1.6130	-1.9911
	-0.4258	-0.8466	-1.0215	-1.4422
	-0.0419	-0.4073	-0.6375	-1.0030
	-0.3801	-0.8491	-0.9758	-1.4448
	0.3390	-0.0591	-0.2567	-0.6548
	-0.2265	-0.7046	-0.8222	-1.3003
	-0.1098	-0.4657	-0.7054	-1.0614
	-0.8738	-1.3416	-1.4695	-1.9373
	-0.6858	-1.0271	-1.2815	
	-0.7657	-1.1361	-1.3614	-1.7317
	-0.7936	-1.1837	-1.3892	-1.7794
	-0.4363	-0.7862	-1.0320	
	-0.8315	-1.2499	-1.4271	-1.8455
	-0.1196	-0.4910	-0.7153	-1.0866
	-0.5953	-1.0222	-1.1910	-1.6179
	-0.3303	-0.6429	-0.9260	-1.2385
	0.1228	-0.1365	-0.4729	-0.7322
	-0.8702	-1.2399	-1.4659	-1.8355
	-1.4695	-1.9617	-2.0652	-2.5573
Ave	-0.4523	**-0.8270**	-1.0475	-1.4151
Min	-1.4695	**-1.9617**	-2.0652	-2.5573
Max	0.3390	**-0.0591**	-0.2567	-0.6548